Thermal Fault Detection and Severity Analysis of Mechanical and Electrical Automation Equipment

Yan Cheng

School of Mechatronics Engineering, Zibo Vocational Institute, Zibo 255314, China

Corresponding Author Email: 11304@zbvc.edu.cn

ABSTRACT

Effectively diagnosing thermal faults in key parts of mechanical and electrical automation equipment before they become too serious is of crucial importance for the safe and continuous operation of these equipment. However, existing algorithms are not able to establish stable connections among sensors, so the overall control of thermal faults is not ideal enough. To cope with this issue, this paper aims to study the thermal fault detection of mechanical and electrical automation equipment and analyze the severity of the faults. At first, this paper studied the heterogeneous Multi-Sensor Information Fusion (MSIF) problem of sensors installed in key parts inside the mechanical and electrical automation equipment, and proposed a MSIF algorithm based on the D-S evidential theory. Then, the paper evaluated the influence of damages caused by thermal faults on the different parts of the equipment, providing evidences for the installation of sensors in key parts of the equipment. At last, experimental results proved the effectiveness of the proposed algorithm, and the thermal fault detection results were attained.

1. INTRODUCTION

The electromechanical integration and automation of mechanical equipment has received increasing attention in real applications [1-4]. Faults caused by long-term service, poor heat dissipation environment, load changes, or manual mis-operations to the equipment need to be processed in a timely manner, so that the production efficiency of the equipment could be guaranteed [5-10]. The faults of mechanical and electrical automation equipment (hereinafter referred to as "equipment" for short) mainly include three types: switch fault, short circuit fault, and grounding fault. Faults of all three types have the phenomena of intense heat release, device burnout, and open fire [11-15]. Equipment generally has several key parts; the abnormal temperature rise in these key parts must be discovered and handled in time [16-20], therefore, effectively diagnosing thermal faults in key parts of the equipment before they become too serious is of crucial importance for the safe and continuous operation of the equipment.

To reduce power consumption of circuit and increase output swing, Zhao et al. [21] proposed a 2-fold structure for controlled voltage and current parts in the shared circuit of wireless sensor units; for system design requirements, the paper gave a detailed discussion on the overall structure of temperature measurement nodes and the design parameters of the chip, devised the general architecture of the chip, and performed simulation experiment on the steady temperature rise of the heated electric field. To accurately evaluate the operation state of dry-type electric reactor, improve the diagnosis level of equipment faults, and ensure the safe and reliable operation of power grid, Li et al. [22] analyzed the structure of dry-type electric reactor and analyzed its abnormal faults based on infrared temperature measurement technology; then, the paper summarized the abnormal heating faults in

high-voltage wiring board, neutral wiring board, grounding bar, post insulator stander, and the wiring board of DC filter reactor; after that, according to relevant test data and standards, the paper analyzed the causes of heating faults in different parts and gave targeted countermeasures. According to the structure of switch cabinet and the features of heating faults, Su et al. [23] employed the heat transfer theory to analyze the internal heat transfer features of heating faults in the switch cabinet, and established a mathematical model in software FLUENT for simulation verification, the paper provided theoretical evidences for the diagnosis of heating faults inside the cabinet. Matsui et al. [24] proposed to apply the IR-OBIRCH method to fault location in semiconductor devices and locate the faults by observing the current changes caused by laser heating.

In an environment with too-high or too-low ambient temperature, thermal fault diagnosis algorithms such as inter-phase temperature method or relative temperature method can easily trigger the alarm threshold, resulting in missing or false alarm. Meanwhile, the sensors couldn't establish stable connections, so the overall control of thermal faults is not ideal enough. To cope with this issue, this paper studied the thermal fault detection of mechanical and electrical automation equipment and analyze the severity of the faults. In the second chapter, this paper studied the heterogeneous MSIF problem of sensors installed in key parts inside the equipment, and proposed a MSIF algorithm based on the D-S evidential theory. The third chapter evaluated the influence of damages caused by thermal faults on the different parts of the equipment, which provided evidences for the installation of sensors in key parts of the equipment. At last, experimental results proved the effectiveness of the proposed algorithm, and the thermal fault detection results were attained.

2. THERMAL FAULT DETECTION OF MECHANICAL AND ELECTRICAL AUTOMATION EQUIPMENT
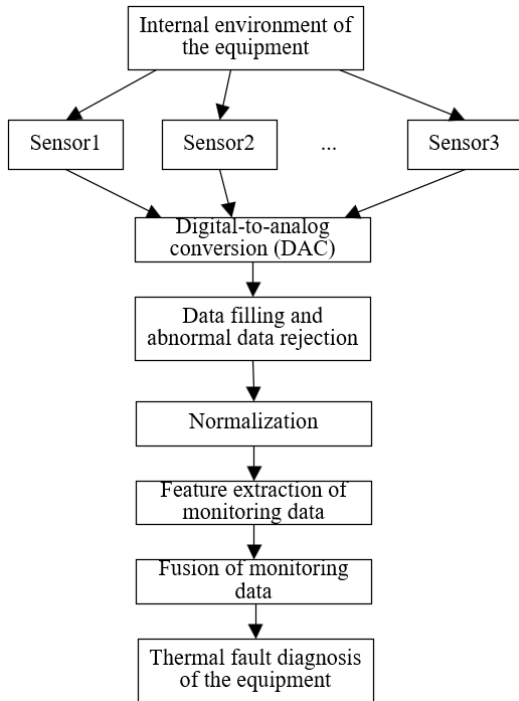

Figure 1. Flow of the MSIF algorithm

In order to give comprehensive descriptions of the states of thermals faults of monitored equipment via the calculation of multi-sensor data, the adopted algorithm must have more advantages than description algorithms that rely on the data collected by single-type sensors. After many years of theoretical research and practical application, the stability and reliability of MSIF algorithm have been improved gradually, and now it could be applied to thermal fault detection and severity diagnosis of mechanical and electrical automation equipment. Figure 1 gives the flow of the MSIF algorithm.

Under normal conditions, multiple heterogeneous or homogeneous sensors are installed in the key parts of the equipment, since there're great differences in the attributes of information collected by the sensors, before the fusion of the collected information, data filling, abnormal data rejection, data normalization and other processing should be carried out to facilitate system recognition.

For the MSIF of data measured by homogeneous sensors, the fusion results can only describe a single environmental factor in the internal environment of the equipment. To judge the overall environment, the information of other environmental factors should be combined as well, therefore, this paper studied the MSIF of data measured by heterogeneous sensors installed in key parts of the equipment.

The main idea of MSIF of data collected by heterogeneous sensors is that: at first, the features of various types of data are evaluated to judge the importance of thermal faults in the equipment; then, the data are weighted and fused to attain the fusion results. The D-S evidential theory is often applied to heterogeneous sensor data fusion modeling, in order to make the theory less subjective and improve the effect of data fusion, this paper improved it. At first, the sources of original evidences were subject to conflict analysis, then the improved D-S evidential theory was applied to the fusion of the evidence sources that have conflicts, and the conventional D-S combination rules were applied to the fusion of the evidence sources that do not have conflict. Figure 2 gives the flow of MSIF algorithm based on the D-S evidential theory.

By referring to the cosine values of the angle, the differences in the directions of two vectors could be described, in this way, the same idea could be applied to the measurement of the differences between two evidence vectors in the D-S evidential theory.

If two evidences n_i and n_j are independent of each other, the cosine similarity r_{ij} of n_i and n_j can be calculated by Formula 1:

$$r_{ij} = cos_{n_i n_j} = \frac{(n_i n_j)}{|n_i| \cdot |n_j|} \tag{1}$$

According to above formula: when $r_{ij}=1$, the two evidence vectors coincide, which means that they are exactly the same. When r_{ij} decreases, the angle between the two evidence vectors increases, indicating the difference between the two, namely the conflict between them increases. When the angle between the two evidence vectors is 90°, namely when $r_{ij}=0$, it indicates that there's no correlation between the two. When the angle between the two evidence vectors is 180°, namely when $r_{ij} = -1$, it means that the two are negatively correlated, that is, the relationship between them is a complete conflict. The following formula can calculate the average evidence similarity which is used to describe the similarity between evidences:

$$\bar{R} = \begin{bmatrix} \bar{R}_1 \\ \bar{R}_2 \\ \vdots \\ \bar{R}_M \end{bmatrix} \tag{2}$$
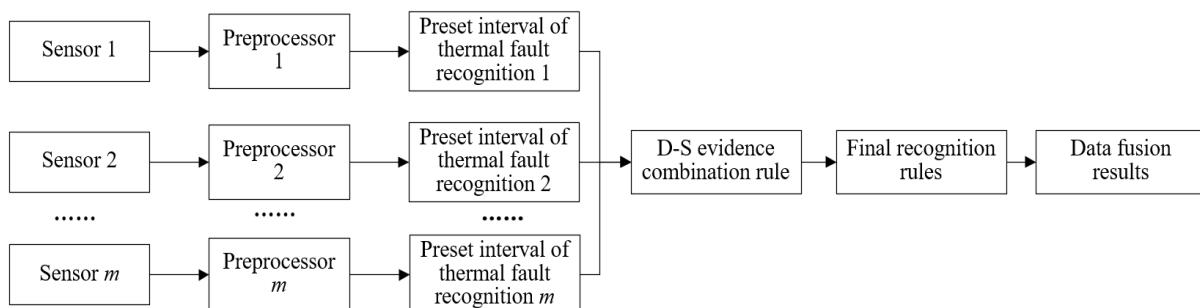

Figure 2. Flow of MSIF algorithm based on D-S evidential theory

where,

$$\bar{R}_i = \frac{\sum_{j=1}^{L} r_{ij}}{L} \qquad (3)$$

If the average similarity is greater than the preset threshold, it can be judged that the degree of difference of evidences is relatively small. If it is less than the preset threshold, it can be judged that there is a certain conflict between the evidences. The redistribution of focal element weights of the information data of heterogeneous sensors was realized by introducing a distance function, and the conflicting evidences of evidence sources were replaced by the average evidence. At last, a confidence matrix was constructed to complete the MSIF of heterogeneous sensors. Based on each evidence, the average value of the *l*-th focal element was calculated as follows:

$$\bar{n}_l = \frac{n_1 + n_2 + ... + n_m}{m} \qquad (4)$$

Assuming: n_{ij} represents the basic probability function value of the *i*-th evidence with respect to the *j*-th focal element, then, the distance from the evidence to the average value of the focal element was calculated:

$$\delta_i = d^{-|n_{i1} - \bar{n}_1|} + d^{-|n_{i2} - \bar{n}_2|} + ... + d^{-|n_{ij} - \bar{n}_j|}, i = 1, 2, ..., m \qquad (5)$$

According to above formula, the lower the degree of similarity between two evidences, the greater the value of δ_i; the higher the degree of similarity between two evidences, the smaller the value of δ_i; the weight of each evidence could be calculated by Formula 6:

$$\theta_i = \frac{\delta_i}{\sum_{i=1}^{m} \delta_i} \qquad (6)$$

Assuming: θ_i represents the weight of the *i*-th evidence and it satisfies $\Sigma^n_{i=1}\theta_i=1$, then the average value of the new evidence with respect to the focal element was calculated by the following formula:

$$\bar{n}' = \theta_i n_i \qquad (7)$$

Assuming: n_{ij} represents the basic probability distribution value of evidence *i* with respect to focal element *j*, then the constructed confidence matrix *N* can be expressed as Formula 8:

$$N = \begin{bmatrix} N_1 \\ N_2 \\ \vdots \\ N_m \end{bmatrix} = \begin{bmatrix} n_{11} & n_{12} & \cdots & n_{1n} \\ n_{21} & n_{22} & \cdots & n_{2n} \\ \vdots & \vdots & \cdots & \vdots \\ n_{m1} & n_{m2} & \cdots & n_{mn} \end{bmatrix} \qquad (8)$$

Then each row of *N* was added to get:

$$n_{i1} + n_{i2} + \cdots + n_{in} = 1, (i = 1, 2, ..., m) \qquad (9)$$

The *i*-th row of *N* was transposed and multiplied by the *j*-th row to attain:

$$N_i^T \times N_j = [n_{i1}, n_{i2}, \cdots, n_{in}]^T \cdot [n_{j1}, n_{j2}, \cdots, n_{jn}] \qquad (10)$$

The newly attained matrix *X* can be expressed by Formula 11:

$$X = \begin{bmatrix} n_{i1} \times n_{j1} & n_{i1} \times n_{j2} & \cdots & n_{i1} \times n_{jn} \\ n_{i2} \times n_{j1} & n_{i2} \times n_{j2} & \cdots & n_{i2} \times n_{jn} \\ \vdots & \vdots & \cdots & \vdots \\ n_{in} \times n_{j1} & n_{in} \times n_{j2} & \cdots & n_{in} \times n_{jn} \end{bmatrix} \qquad (11)$$

According to formula 11, the fusion result of evidence *i* and evidence *j* was the product of elements on the diagonal of the new matrix *X*, and the uncertainty coefficient of fusion result was the sum of all other elements in *X*, that is in formula 12:

$$L' = \sum_{t \neq w} n_{it} \times n_{jw} (t, w = 1, 2, ..., n) \qquad (12)$$

Finally, using Formula 13, the information data of multiple heterogeneous sensors were fused:

$$n_j = \frac{N_{ij}}{1 - L'} \qquad (13)$$

The construction of basic probability distribution function is a difficulty in the implementation of D-S evidential theory for MSIF of heterogeneous sensors, the mapping of the sensor information data samples is usually realized depending on the experience of experts. According to the features of the internal environment of the equipment, in this paper, the basic probability distribution function was constructed based on the membership function of fuzzy set. Also, according to the main environmental factors such as temperature and humidity of the equipment model and the features of current in the equipment, this paper chose the triangular function and trapezoidal function as the membership functions to establish the basic probability distribution function, and divided it into three states: suitable, low, and high.

Assuming: $F(X)$, $F(Y)$ and $F(Z)$ represent thermal fault recognition frameworks of the equipment; the evidences are temperature, humidity, and equipment current; $n(1)$, $n(2)$ and $n(3)$ represent the basic probability distribution functions of the three kinds of evidences, then, the basic probability distribution function $n_i(F_i)$ of the three kinds of evidences is given by Formula 14:

$$n_i(F_i) = \frac{\lambda_i(F_j)}{\sum_j \lambda_i(F_j) + (1 - \beta_i)(1 - \gamma_i)} \qquad (14)$$

Correspondingly, the uncertainty description $n_i(\Psi_i)$ can be expressed by Formula 15:

$$n_i(\Psi) = 1 - n_i(F_1) - n_i(F_2) - n_i(F_3) \qquad (15)$$

Assuming: $\lambda_i(F_i)$ represents the membership function of related BOEs (body of evidence) of equipment thermal fault recognition; β_i represents the difference between the maximum value and the second maximum value of the membership degrees of BOEs related to thermal fault recognition; γ_i represents the variance of the membership degrees of the remaining BOEs after the maximum membership degree has been eliminated; q_i represents the average value of the membership degrees of the remaining BOEs after the maximum membership degree has been eliminated, then their expressions are given by the following formulas:

$$\beta_i = \lambda_i(F_l) - max\{\lambda_i(F_j)\}, j \neq l \tag{16}$$

$$\lambda_i(F_l) = max\{\lambda_i(F_j)\} \tag{17}$$

$$\gamma_i = \sqrt{\frac{1}{L-1}\sum_{j \neq l}^{l}\left[\lambda_i(F_j) - q_i\right]^2} \tag{18}$$

$$q_i = \sum_{j \neq l}^{l}\frac{1}{L-1}\lambda_i(F_j) \tag{19}$$

3. SEVERITY ANALYSIS OF THERMAL FAULT DAMAGES OF THE EQUIPMENT

The severity evaluation of thermal fault damages of the equipment is to evaluate the influence of thermal faults on the damages in different parts of the equipment based on the high-temperature tolerance features of the key parts of the equipment, it can provide evidences for the installation of sensors in key parts of the equipment. The texts below introduced the evaluation indicators of the severity of thermal fault damages of the equipment.

Assuming: ρ represents the duration of thermal fault; I represents the current amplitude of the equipment; $I_{HT}(\rho)$ represents the current amplitude of the equipment corresponding to duration time ρ on the high-temperature tolerance curve, then the severity index of thermal faults R_d could be defined by Formula 20, which can describe the severity of thermal fault damages in key parts of the equipment:

$$R_d = \frac{1-I}{1-I_{HT}(\rho)} \tag{20}$$

When thermal fault damage occurs to a certain part of the equipment, if the equipment current is smaller than I_{min} and the time duration is longer than ψ_{max}, the equipment will operate abnormally. If the equipment current is between I_{min} and I_{max} and the duration is between ψ_{min} and ψ_{max}, the equipment is in an uncertain state, otherwise it runs normally. Based on the generalized high-temperature tolerance curve of key parts of the equipment, it's defined that the duration severity index of thermal fault damage of the equipment is represented by QWR, the current amplitude severity index of thermal fault damage of the equipment is represented by NJF, and the comprehensive severity index of thermal fault damage of the equipment is represented by $NQWR$, their expressions are given by the formulas 21-23. Then, the severity of the thermal fault damage of the equipment was quantified, the greater the influence, the more serious the thermal fault. Assuming: Z represents the duration and amplitude of thermal fault damage of the equipment, G represents the mapping function, in order to evaluate the severity of the thermal fault damage of the equipment based on the weight function, at first, an influence degree function E was constructed, as given by Formula 24.

$$QWR(V) = \begin{cases} 0, \psi > \psi_{max} \\ (\psi_{max} - \psi) \times \left(\dfrac{100}{\psi_{max} - \psi_{min}}\right), \\ 100, \psi < \psi_{min} \end{cases} \tag{21}$$

$$\psi_{min} \leq \psi \leq \psi_{max}$$

$$NJF(V) = \begin{cases} 0, V > V_{max} \\ (V_{max} - V) \times \left(\dfrac{100}{V_{max} - V_{min}}\right), V_{min} \leq V \leq V_{max} \\ 100, V < V_{min} \end{cases} \tag{22}$$

$$NQWR(V,P) = \frac{NJF(V) \times QWR(P)}{100} \tag{23}$$

$$E = G(Z), 0 \leq E \leq 1 \tag{24}$$

For the relationship between the influence degree of thermal fault damage and high-temperature duration and equipment current amplitude, it has the features of changing faster in the middle and slower at both ends. Assuming σ and φ are control parameters, then there is:

$$b = \frac{1}{1+d^{\sigma - \phi * a}} \tag{25}$$

According to the interval statistics of duration of equipment thermal fault damage and the equipment current amplitude of thermal fault, the probability of thermal fault occurrence is relatively high within the interval of a high-temperature duration between 5-10 minutes and an equipment current amplitude between 20-30A. Therefore, in terms of the influence of high-temperature duration, it's considered that the influence degree of a high-temperature duration of 5min is 0.05, and the influence degree of a high-temperature duration of 10min is 0.95; while in terms of the influence of equipment current amplitude, the influence degree of an equipment current amplitude of 20A is 0.15, and the influence degree of an equipment current amplitude of 30A is 0.95, thus, the influence degree function about the high-temperature duration, equipment current amplitude, and the thermal fault damage event of the equipment can be expressed as:

$$PE = \frac{1}{1+d^{4-9P}} \tag{26}$$

$$NE = \frac{1}{1+d^{-3+8V}} \tag{27}$$

$$E = \frac{\sqrt{PE^2 + NE^2}}{2} \tag{28}$$

4. EXPERIMENTAL RESULTS AND ANALYSIS

To overcome the influence of the internal temperature changes of the equipment on the thermal fault detection results, this paper eliminated some uncertain factors of the internal temperature changes of the equipment, and gave the criterion of relative temperature difference of some equipment in the experiment (Table 1), so that the detection results of thermal faults could be more accurate and reliable.

For a specific type of thermal faults, the sensor points of the heterogeneous multi-sensor monitoring system of the equipment were set, and the specific conditions of the sensor points of the corresponding equipment lines are given in Table 2. Based on this, changes in the collected signal of each sensor node of the sensor monitoring system with the location of thermal faults in the equipment lines could be inferred further.

After attaining the number of intersections of the threshold, the changes in the observability of sensors when thermal faults occur at several key parts in the equipment lines could be inferred. Since within the preset interval of thermal fault recognition of each sensor, the observability of sensor nodes remains unchanged, the observability of sensor nodes when thermal faults occur at several parts in the equipment lines could be used to characterize the observability in case of continuous thermal faults in the equipment lines.

Then, based on the constructed observability matrix of the heterogeneous multi-sensor monitoring system, the optimal configuration scheme of sensor monitoring points was solved using various algorithms, and the observation ability function values of the thermal fault monitoring system containing 18 sensors were obtained, as shown in Table 3. Table 4 gives the configuration of monitoring points of the sensor system, which includes four aspects: node configuration result, observability constraint, observation ability, and reliability. According to the table, the solution obtained by multi-objective Particle Swarm Optimization (PSO) could meet the observability

constraints on the premise of considering the continuity and integrity of the lines, and the obtained configuration scheme is conducive to further data fusion.

One group of data in the local MSIF results obtained in chapter 2 was taken as an example to perform the fusion experiment (temperature: 45.6°C, humidity: 3.5%, equipment current 21A), then, based on the constructed membership function, the fuzzy membership of the eigenvalue parameters of the data collected by various types of sensors can be calculated, and the results are shown in Table 5.

Table 6 shows the basic belief assignment function values corresponding to various types of sensors, these values describe the support degree of the information of internal environmental factors of the equipment collected by heterogeneous multi-sensors to the thermal fault recognition framework. According to the table, the preset threshold was lower than the average similarity between evidences, indicating negative correlation between evidences, namely the conflict degree hadn't reached an unacceptable level. Table 7 lists the results of MSIF.

Table 1. Criterion of relative temperature difference of some equipment

Equipment No.	Relative temperature difference %		
	General thermal fault	Major thermal fault	Emergency thermal fault
1	≥41	≥82	≥91
2	≥45	≥84	≥95
3	≥42	≥88	≥94
4	≥48	≥83	≥93
5	≥52	≥86	≥95
6	≥42	≥81	≥92
7	≥47	≥85	≥95

Table 2. Number of line points of the sensor system

Line No.	Number of points	Line No.	Number of points	Line No.	Number of points
1	15	11	47	21	22
2	13	12	5	22	17
3	21	13	23	23	11
4	8	14	19	24	16
5	24	15	15	25	10
6	26	16	22	26	5
7	7	17	17	27	9
8	22	18	13	28	25
9	13	19	8	29	22
10	9	20	8	30	13

Table 3. Observation ability function of the sensor system

Node No.	Observation ability	Node No.	Observation ability	Node No.	Observation ability
1	0.0265	7	0.1486	13	0.0415
2	0.0147	8	0.0723	14	0.2962
3	0.1852	9	0.2759	15	0.2184
4	0.2729	10	0.3394	16	0.3629
5	0.0748	11	0.0326	17	0.3741
6	0.2325	12	0.2748	18	0.3052

Table 4. Configuration of measuring points of the sensor system

	Multi-objective PSO	Conventional PSO	Conventional genetic algorithm	Conventional ant colony optimization
Configuration result	3, 5, 8, 17	2, 7, 10, 13	6, 11, 18	8, 12, 15, 17
Observability constraint	Satisfy	Not satisfy	Not satisfy	Satisfy
Observation ability	0.7481	0.6329	0.6852	0.6108
Reliability	65.12%	67.43%	62.84%	67.35%

Table 5. Fuzzy membership degree corresponding to data collected by various types of sensors

	Temperature	Humidity	Equipment current
X	1	5	3
Y	0.325	0.317	0.396
Z	0.674	0.629	0.715

Table 6. Basic belief assignment function

	Temperature	Humidity	Equipment current
$n(X)$	3	1	4
$n(Y)$	0.285	0.25	0.157
$n(Z)$	0.384	0.492	0.486
$n(D)$	0.357	0.331	0.284

Table 7. Results of MSIF

	Temperature	Humidity	Equipment current	Fusion result
$n(X)$	5	2	4	1
$n(Y)$	0.281	0.268	0.139	0.052
$n(Z)$	0.374	0.495	0.418	0.826
$n(D)$	0.317	0.359	0.262	0.168

Judging from the data in Table 7, among focal elements X, Y and Z, the confidence level of Z was the highest. According to the original data of this fusion: temperature 45.6°C, humidity 3.5%, equipment current 21A, and combining with the preset interval of thermal fault recognition of X (temperature 40°C-95°C, humidity 10%-15%, equipment current 20A~30A), it can be judged that the fusion results of MSIF using the fusion algorithms adopted in this paper could basically meet the expectations.
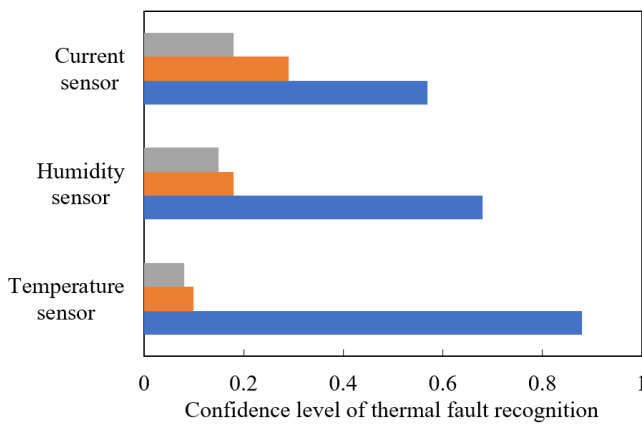

Figure 3. Changes before and after data fusion

In order to intuitively reflect the changes before and after MSIF, this paper employed MATLAB to display the fusion results based on the column diagram, as shown in Figure 3, after MSIF for multiple times, the uncertainty of equipment thermal fault detection decreased gradually, the confidence level of thermal fault recognition increased gradually, and all involved evidences converged toward a certain direction. Based on the thermal fault detection decision-making formula proposed in the D-S evidential theory, after fully referring to the real examples of equipment thermal faults, in this paper, the threshold value was set to be 1.5, and the final judgement was that the equipment had a great probability of thermal faults. Thus, it can be known that, the multi-cycle fusion processing of the data collected by multiple sensors could effectively avoid the inaccuracy of thermal fault detection results caused by one-time collection of single-type data, enhance the complementarity of information, and reduce the detection errors.

5. CONCLUSION

This paper studied the thermal fault detection of mechanical and electrical automation equipment and analyzed the severity of thermal fault damages. At first, the information fusion of heterogeneous multi-sensors installed in key parts of the equipment was discussed, and a MSIF algorithm had been proposed based on the D-S evidential theory. Then, the influence of thermal fault damages on different parts of the equipment was evaluated, which could provide evidences for the installation of sensors in key parts of the equipment. Combining with experiment, this paper proposed criterion of relative temperature difference for some equipment, which could make the detection results of thermal faults more accurate and reliable. After that, this paper gave the specific numbers of sensor points in each equipment line, and several algorithms were employed to solve the optimal configuration scheme of sensor monitoring points based on a constructed observability matrix of the heterogeneous multi-sensor monitoring system, the values of each observation ability function of the thermal fault monitoring system containing 18 sensors were attained, and the obtained configuration scheme was conducive to further data fusion. Finally, this paper also gave the changes before and after data fusion of various types of sensors, and the results had proved that the multi-cycle fusion processing of the data collected by multiple sensors could effectively avoid the inaccuracy of thermal fault detection results caused by one-time collection of single-type data.

REFERENCES

[1] Zhang, M.M. (2022). Numerical analysis and optimization of heat dissipation of mechanical automation equipment based on thermal model. International Journal of Heat and Technology, 40(1): 311-318. https://doi.org/10.18280/ijht.40013

[2] Lavrikov, S.A., Kotsar, M.L., Lapidus, A.O., et al. (2014). Automation of high-purity zirconium production from wastes and recycled materials on industrial equipment at the Chepetskii mechanical plant. Atomic Energy, 115(6): 427-432. https://doi.org/10.1007/s10512-014-9806-3

[3] Zhang, N., Chen, L., Li, T. (2013). Study on mechanical automation with airborne guiding ammunition automatic testing equipment development. Applied Mechanics and Materials, 387: 280-283. https://doi.org/10.4028/www.scientific.net/AMM.387.280

[4] Zhu, P. (2021). Safety control of mechanical design automation equipment with computer aid. Journal of Physics: Conference Series, 1992(2): 022041. https://doi.org/10.1088/1742-6596/1992/2/022041

[5] Hou, N., Ding, N., Qu, S., et al. (2022). Failure modes, mechanisms and causes of shafts in mechanical equipment. Engineering Failure Analysis, 136: 106216. https://doi.org/10.1016/j.engfailanal.2022.106216

[6] Duan, C., Makis, V., Deng, C. (2020). A two-level Bayesian early fault detection for mechanical equipment subject to dependent failure modes. Reliability Engineering & System Safety, 193: 106676. https://doi.org/10.1016/j.ress.2019.106676

[7] Williamson, T., Ellis, L., Fletcher, J. (2018). Challenges of repairing small ageing dams caused by the deterioration and failure of hydro mechanical equipment. In Twenty-Sixth International Congress on Large Dams: Vingt-Sixième Congrès International des Grands Barrages, pp. 515-531.

[8] Sun, Y. (2016). Analysis of mechanical equipment failure based on improved AFSA-SVM. International Journal of Control and Automation, 9(7): 125-132. https://doi.org/10.14257/ijca.2016.9.7.12

[9] Lawrence, R., Zimmer, D. (2016). Mitigating mechanical failures in ASD-driven equipment: Proven methods. IEEE Industry Applications Magazine, 22(6): 48-56. https://doi.org/10.1109/MIAS.2015.2459092

[10] Trebuňa, F., Šimčák, F., Bocko, J., Trebuňa, P. (2010). Failure analysis of mechanical elements in steelworks equipment by methods of experimental mechanics. Engineering Failure Analysis, 17(4): 787-801. https://doi.org/10.1016/j.engfailanal.2009.10.011

[11] Zhao, Y., Yu, M., Sun, J., et al. (2022). Electrical failure mechanism in stretchable thin-film conductors. ACS Applied Materials & Interfaces, 14(2): 3121-3129. https://doi.org/10.1021/acsami.1c22447

[12] Song, P., Liu, J., Wang, F., Sun, X. (2021). The study of inspection on thin film resistance strain gauge contact failure by electrical excitation thermal-wave imaging. IEEE Transactions on Industrial Electronics, 69(6): 6288-6297. https://doi.org/10.1109/TIE.2021.3088368

[13] Peruzzi, R. (2021). Forensic engineering investigation of electrical and electronic causes of an industrial equipment failure. Journal of the National Academy of Forensic Engineers, 38(2): 21-32. https://doi.org/10.51501/jotnafe.v38i2.812

[14] Resende, J., Papanastasiou, D.T., Moritz, D.C., Fontanals, N., Jiménez, C., Muñoz-Rojas, D., Bellet, D. (2022). Time of failure of metallic nanowire networks under coupled electrical and thermal stress: Implications for transparent electrodes lifetime. ACS Applied Nano Materials, 5(2): 2102-2112. https://doi.org/10.1021/acsanm.1c03821

[15] Zhang, G., Zhang, L., Li, M., He, X., Li, L., Duan, M. (2021). An evaluation method for electrical contact failure based on high-frequency impedance model. IEEE Transactions on Components, Packaging and Manufacturing Technology, 11(4): 579-588. https://doi.org/10.1109/TCPMT.2021.3067653

[16] Cheng, Y. (2021). Thermal fault diagnosis of transmission system in automatic production machinery and equipment and reliability analysis. International Journal of Heat and Technology, 39(6): 1713-1720. https://doi.org/10.18280/ijht.390603

[17] Li, S.T., He, J.Q., Lin, J.J., et al. (2015). Electrical-thermal failure of metal–oxide arrester by successive impulses. IEEE Transactions on Power Delivery, 31(6): 2538-2545. https://doi.org/10.1109/TPWRD.2015.2506785

[18] Luo, Y.Y., Liu, X.Y., Hao, J., et al. (2016). Research on thermal fatigue failure mechanism of aviation electrical connectors. Acta Armamentarii, 37(7): 1266-1274. https://doi.org/10.3969/j.issn.1000-1093.2016.07.015

[19] Qu, Z.H. (2021). Thermodynamic analysis and calculation of the drying and heating system of automatic stirring equipment. International Journal of Heat and Technology, 39(6): 1871-1877. https://doi.org/10.18280/ijht.390622

[20] Luo, Y.Y., Wang, Z., Li, X.N., Liu, L. (2014). Accelerated thermal cycling test and failure analysis of electrical connectors. Acta Armamentarii, 35(11): 1908-1913. https://doi.org/10.3969/j.issn.1000-1093.2014.11.024

[21] Zhao, Y., Zhuang, J., Ye, Z., Qian, Z., Peng, F. (2021). Simulation of steady-state temperature rise of electric heating field of wireless sensor circuit fault current trigger. Journal of Sensors, 2021: 8359504. https://doi.org/10.1155/2021/8359504

[22] Li, Y., Li, Q., Liu, Z., Chen, Q. (2021). Diagnosis and analysis of abnormal heating fault for 35kV dry air core reactor. In 2021 IEEE 5th Advanced Information Technology, Electronic and Automation Control Conference (IAEAC), Chongqing, China, pp. 431-434. https://doi.org/10.1109/IAEAC50856.2021.9390877

[23] Su, Y., Xie, Z., Li, L., Lu, Y., Wang, J. (2020). Analysis of internal heat transfer characteristics of high voltage switch cubicle heating fault. IOP Conference Series: Earth and Environmental Science, 508(1): 012173. https://doi.org/10.1088/1755-1315/508/1/012173

[24] Matsui, T., Hayashi, H., Kawashima, T., Murakami, Y., Hozumi, N., Matsumoto, T. (2020). Nondestructive fault localization of semiconductor devices with ultrasound heating. In 2020 International Symposium on Electrical Insulating Materials (ISEIM), Tokyo, Japan, pp. 470-473.